AutoGaitA: A versatile quantitative framework for kinematic analyses across species, perturbations and behaviours

Mahan Hosseini[1], Ines Klein[2], Veronika Wunderle[2], Carolin Semmler[2], Taylan D. Kuzu[2], Ann-Kathrin Kramer[2], Marianna Tolve[2,3], Vlad Mardare[3], Ana Galvao[2], Moritz Haustein[4], Christian Grefkes[5], Tatiana Korotkova[3], Ansgar Büschges[4], Gereon R. Fink[1, 2], Peter H. Weiss[1, 2], Silvia Daun[1, 4]*, Graziana Gatto[2]*

[1] Institute of Neuroscience and Medicine (INM-3), Forschungszentrum Jülich, Germany

[2] Department of Neurology, University Hospital of Cologne, Germany

[3] Institute of Systems Physiology, University Hospital of Cologne, Germany

[4] Institute of Zoology, University of Cologne, Germany

[5] Goethe University Frankfurt and University Hospital, Department of Neurology

*corresponding authors: graziana.gatto@uk-koeln.de, s.daun@fz-juelich.de

Abstract

Individual behaviours require the nervous system to execute specialised motor programs, each characterised by unique patterns of coordinated movements across body parts. Deep learning approaches for body-posture tracking have facilitated the analysis of such motor programs. However, translating the resulting time-stamped coordinate datasets into meaningful kinematic representations of motor programs remains a long-standing challenge. We developed the versatile quantitative framework AutoGaitA (Automated Gait Analysis), a Python toolbox that enables comparisons of motor programs at multiple levels of granularity and across tracking methods, species and behaviours. AutoGaitA allowed us to demonstrate that flies, mice, and humans, despite divergent biomechanics, converge on the age-dependent loss of propulsive strength, and that, in mice, locomotor programs adapt as an integrated function of both age and task difficulty. AutoGaitA represents a truly universal framework for robust analyses of motor programs and changes thereof in health and disease, and across species and behaviours.

Introduction

Animals and humans employ an impressively rich array of motor behaviours, such as grooming, swimming or walking, each requiring coordinated neural activity across the nervous system to execute the appropriate motor program[1,2]. Individual motor programs are executed with redundant kinematic solutions, which arise from distinct combinations of joint positions, angles and velocities[3] and operate within species-specific biomechanical constraints[1,2]. Consequently, the kinematic outputs of even seemingly simple motor programs, such as walking, exhibit tremendous variability, which complicates deciphering the underlying neural code.

Advances in deep-learning methods, such as DeepLabCut (DLC[4]) and SLEAP[5], have considerably improved our ability to track body landmarks across behavioural tasks and species. Nevertheless, no universal framework currently exists to coalesce these time-stamped body coordinates into meaningful representations of motor programs. Current analysis methods rely on commercial software (e.g., DigiGait, Motorater, Theia3D, SIMI) or custom scripts that are often task- and/or species-specific, limiting their scope. Toolboxes assessing rodent kinematics are task-specific, being constrained to ladder, treadmill (ALMA[6]; PMotion[7]) or beam walking (Forestwalk[8]; Ledged Beam Walking[9]). Further, available analyses provide only basic gait parameters (PMotion, Forestwalk), disease-specific features, e.g. for stroke (PMotion), or complex kinematic extrapolations (ALMA, Ledged Beam Walking). Additionally, although numerous species-specific approaches to gait analysis have been developed for fruit flies[10–13], mice[6,8,9,14,15] and humans[16], no framework exists for cross-species kinematic comparisons.

AutoGaitA (Automated Gait Analysis) provides a versatile framework to standardise the analysis of body coordinates and assess motor programs by comparing kinematic features at different levels of granularity, from individual landmarks to full-body coordination strategies.

Using AutoGaitA, we here demonstrate that fruit flies, mice and humans, despite their divergent biomechanics, share a common age-dependent adaptation strategy: they reduce leg propulsive strength during walking to gain postural stability. Furthermore, we showed that mice employ distinct strategies, defined by age and task difficulty, to preserve the flexibility and robustness of motor execution, suggesting that adaptation strategies emerge as integrative functions of concomitant perturbations.

In sum, AutoGaitA fills a critical gap in the methods currently used to study motor control policies by providing a general-purpose toolbox to assess and compare motor programs and their changes in health and disease across species and behaviours.

Results

A universal framework to analyse rhythmic motor programs at different granularity levels

The heterogeneity of behaviours, model organisms and tracking methods has so far hindered the development of a standardised quantitative framework for the kinematic analysis of motor programs. AutoGaitA addresses this methodological gap by providing a universal framework applicable to any rhythmic behaviour and species. We developed three first-level toolboxes, implementing the same overall workflow to accommodate the diversity of tracking methods (Fig. 1a-c). AutoGaitA DeepLabCut (DLC) and AutoGaitA SLEAP analyse 2D coordinates obtained with DLC[4] or SLEAP[5], respectively. AutoGaitA Universal 3D analyses 3D coordinates tracked with any marker-based or marker-less method.

AutoGaitA's first-level toolboxes transform time series of body coordinates into standardised sets of kinematic outputs. First, AutoGaitA loads the coordinate tables containing the time series of landmark positions and the manually generated annotation tables specifying the timestamps of all behaviour-cycles of interest (Fig. 1a). In this context, a behaviour-cycle (henceforth cycle) defines the simplest instance of a rhythmic behaviour with clearly defined start and end timepoints. For example, a step is the cycle of walking, starting when the foot is lifted off the ground and ending just before the foot is lifted again for the next step. The coordinates are segmented into user-annotated cycles (Fig. 1b), and the segmented data is processed to compute kinematic features: stride (horizontal distance), height (vertical distance), angles, velocities, and accelerations of any user-defined landmark. Next, the segmented data is normalised to bring individual cycles, naturally varying in duration, to a fixed length, making the cycles' kinematics well-suited for comparing and averaging. The generated first-level results consist of image and tabular files containing raw, segmented, normalised and averaged data (Fig. 1c).

The AutoGaitA Group toolbox computes and compares group-level effects after averaging the first-level results of each group (Fig. 1d). Individual kinematic features can be assessed statistically with a permutation test, an ANOVA, and Tukey's test, while more general kinematic patterns can be identified using principal component analyses (PCA). Datasets for each group are provided as tabular files, enabling custom post-hoc analyses when required. The results of group-level comparisons are provided as image and tabular files (Fig. 1e).

To demonstrate AutoGaitA's versatility and applicability, we analysed a published dataset of tracked body landmarks in human subjects performing distinct rhythmic movements (MoVi dataset[17]). Using AutoGaitA, we were not only able to analyse a range of rhythmic behaviours - from running to jumping - but also to cluster the underlying motor programs in PCA space, with similar movements such as walking and running being in closer proximity (Supplementary Note 1, Supplementary Fig. 1).

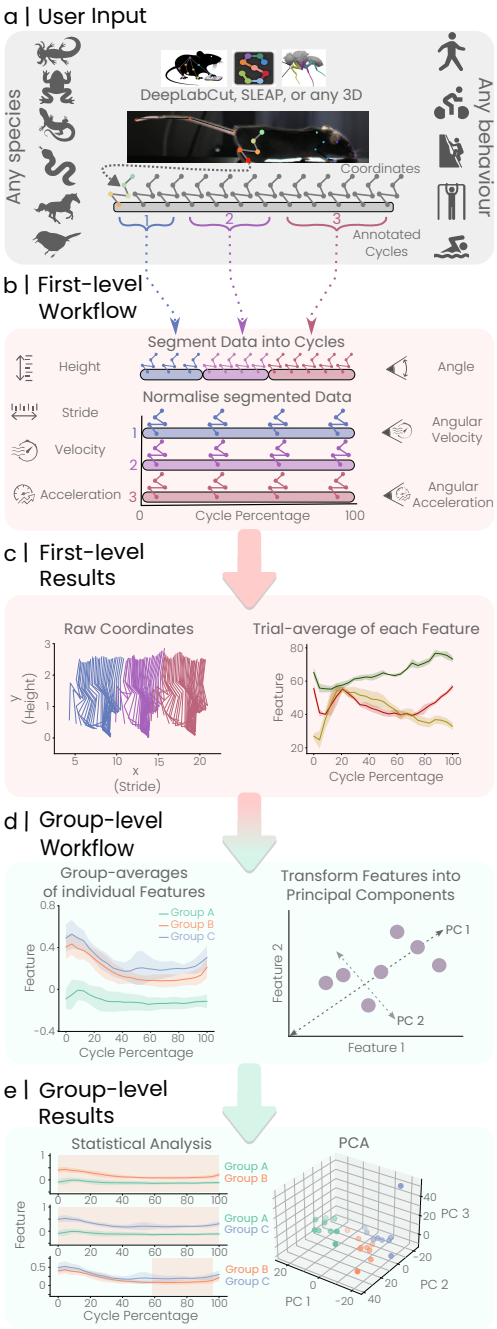

Figure 1 | AutoGaitA's universal framework for the kinematic comparisons of rhythmic behaviours within and across species. **a**, User input. AutoGaitA loads 2D (from DeepLabCut or SLEAP tracking) or 3D (any 3D method) body coordinate data as well as the annotation table storing time information. The AutoGaitA workflow is applicable to any model organisms (e.g. axolotl, salamander, frogs, songbirds) performing a variety of rhythmic behaviours. **b**, First-level workflow. Landmark coordinates are first segmented into cycles based on the annotation table and then normalised. Normalised kinematic features (stride, height, angles, velocities and accelerations) are computed and averaged for each trial. **c**, First-level results. Results are generated as image and tabular files, summarising raw coordinates and kinematic features for each trial after segmentation, normalisation, and averaging. **d**, Group-level workflow. Comparisons of kinematic features among groups are computed via statistical tests and principal component analysis (PCA). **e**, Group-level results. Results of statistical tests (e.g., pair-wise time points of statistical significance and p-values) are provided for each variable tested. PCA results are provided as customisable scatterplots, videos, and tabular files.

94 **Species-specific and convergent strategies of age-dependent motor adaptation**

95 Comparing motor programs across species has long posed a significant challenge due to
96 fundamental biological differences in morphology, biomechanics and size, as well as the
97 heterogeneity of experimental paradigms and posture tracking methods. Leveraging AutoGaitA's
98 ability to analyse coordinate data independently of the model organism and tracking algorithm, we
99 assessed the motor programs underlying walking (henceforth locomotor program) - one of the
100 most fundamental rhythmic behaviours - in flies (*Drosophila Melanogaster*), mice (*Mus*
101 *Musculus*) and humans. DLC was used to track body landmarks in flies walking on a spherical
102 treadmill, mice walking on a 25-mm wide beam, and humans walking on a wide walkway (Fig.
103 2a-c). We focused our analyses on posterior/lower limb landmarks: the thorax-coxa (Th-Cx), the
104 coxa-trochanter (Cx-Tr), the femur-tibia (Fe-Ti), the tibia-tarsus (Ti-Tar), and the tip of the tarsus
105 (Tar) on the fly posterior leg (Fig. 2d); the iliac crest, hip, knee, ankle and middle hindpaw on the
106 mouse hindlimb (Fig. 2e); and the hip, knee, ankle, and midfoot on the human leg (Fig. 2f). We
107 analysed how the kinematic features of these landmarks vary during the step cycle, defined from
108 the beginning of swing (foot is lifted from the ground) to the end of stance (just before the foot is
109 lifted from the ground for the next step) (Fig. 2f). The stick diagrams, illustrating the horizontal
110 (stride) and vertical (height) displacement of the limbs during a step cycle, revealed the divergent
111 kinematics resulting from species-specific biomechanics (Fig. 2g-i).

112 In tethered flies, the proximal Th-Cx and Cx-Tr remained in relatively fixed positions, while
113 the distal Fe-Ti, Ti-Tar and Tar moved, almost synchronously, upward during swing and
114 downward during stance (Fig. 2g,j, Supplementary Fig. 2d). This resulted in all distal joints being
115 maximally flexed at the swing-to-stance transition and maximally extended at the stance-to-swing
116 transition (Supplementary Fig. 2a), suggesting that in flies, distal joints are synergistically

117 coordinated to provide the primary power stroke for forward propulsion of the posterior leg. In
118 mice, the iliac crest remained relatively static throughout the step cycle, the hip moved upward
119 and downward only during swing, the knee and the hindpaw moved upward during swing and at
120 the end of stance and downward during mid-stance, while the ankle exhibited opposite behaviour,
121 moving downward during swing and upward during stance (Fig. 2h,k, Supplementary Fig. 2e).
122 This resulted in the ankle, knee and hip being similarly maximally flexed mid-swing, but diverging
123 in their peak extension, with the ankle and knee being maximally extended at the beginning of
124 stance and the hip at the end of stance (Supplementary Fig. 2b). Together, this kinematic pattern
125 suggests that in mice, the hip provides the initial power stroke, while the relative inversion of ankle
126 and knee positions drives the forward thrust. In humans, the hip oscillated through the step cycle,
127 marking the transitions across swing and stance, the knee moved upward during swing and
128 downward during stance, while the ankle and the midfoot oscillated during swing, and moved
129 upward at the end of stance (Fig. 2i,l, Supplementary Fig. 2f). This resulted in the peak flexion
130 and extension of the knee occurring during swing and of the ankle at the end of stance and
131 beginning of swing (Supplementary Fig. 2c). Taken together, this pattern suggests that in humans,
132 the ankle push-off at the end of stance generates the additional power stroke that, together with the
133 hip-driven oscillations, promotes the forward propulsion. Notably, our kinematic analysis suggests
134 that the generation of propulsive strength relies on coordinated flexion/extension of all distal joints
135 in flies, whereas it requires opposite displacement of knee, ankle and hindpaw in mice, and hip
136 oscillations and ankle push-off in humans. Despite distinct biomechanics, all species converge on
137 landmark velocities increasing along the proximal-to-distal axis (Supplementary Fig. 2g-i). Thus,
138 leveraging the numerous kinematic features assessed by AutoGaitA, we revealed that the
139 mechanisms underlying locomotor programs in hexapedal (flies), quadrupedal (mice) and bipedal

(human) model organisms converge in setting a proximal-to-distal gradient of landmark velocities and diverge in how leg propulsive strength is generated.

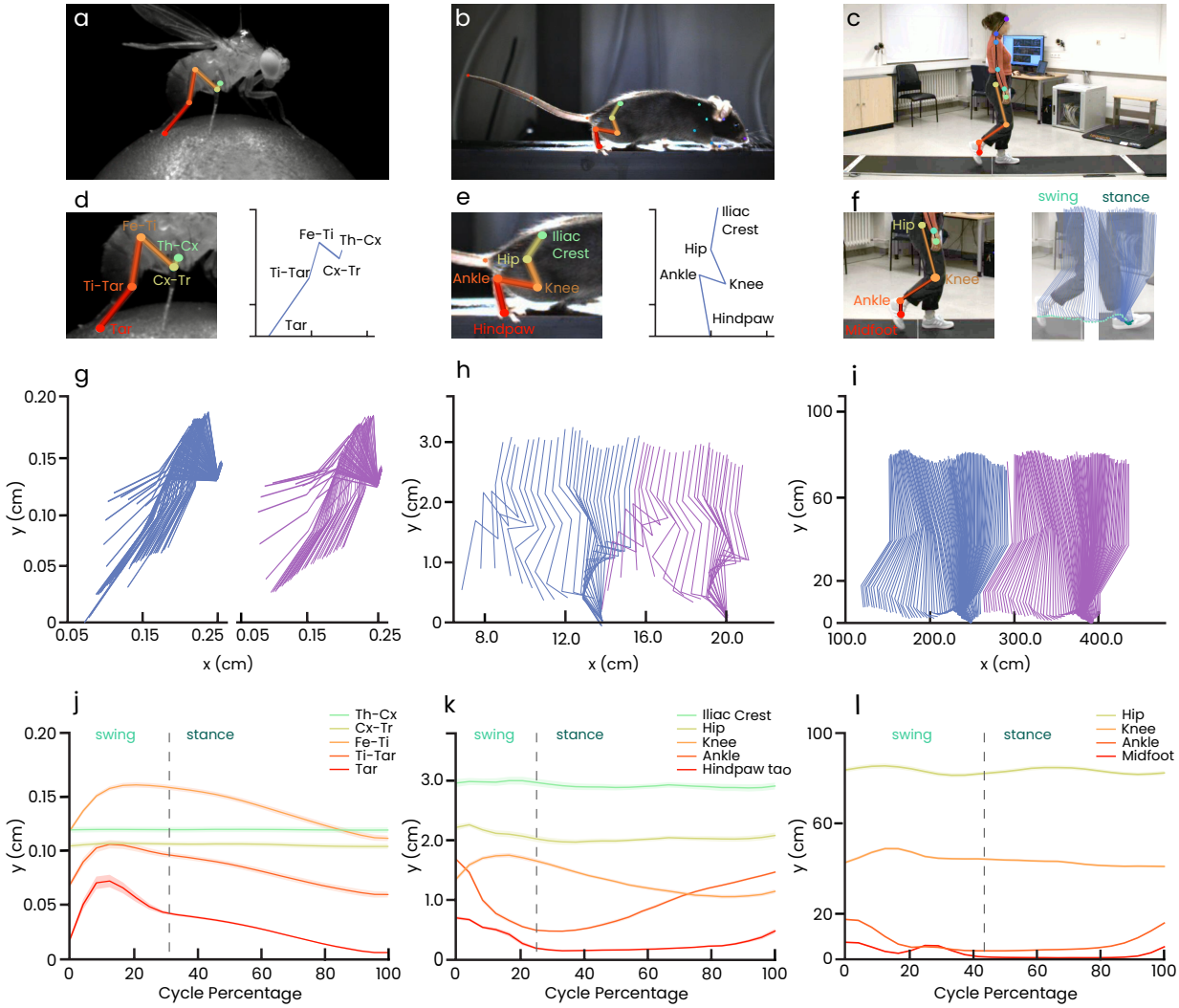

Figure 2 | Divergent and convergent kinematic strategies underlying locomotor programs in flies, mice, and humans. **a-c,** Snapshots of a fly walking on a spherical treadmill (a), a mouse walking on a 25 mm wide beam (b), and a human walking on a walkway (c). **d-f,** Snapshots illustrating the landmarks analysed on the fly posterior leg (d), the mouse hindlimb (e) and the human leg (f). The right panels in d-e illustrate how landmarks translate to the stick diagrams below. The right panel in f depicts a step cycle and its division into swing (toe-off) and stance (toe-down) phases. **g**, Stick diagram illustrating the horizontal and vertical displacements of the fly posterior leg. Note that flies were tethered. **h-i**, Stick diagrams of the mouse hindlimb (h) and human leg (i) for two consecutive steps. **j**, Group-averaged variations in the height of key landmarks of the fly posterior leg throughout the step-cycle showing that all distal joints are moved almost synchronously upward and downward to generate propulsion. **k**, Group-averaged variations in the height of key landmarks of the mouse hindlimb throughout the step-cycle showing that the hip provides the initial power stroke, while the ankle and knee invert their relative heights to generate the subsequent thrust. **l**, Group-averaged variations in the height of key landmarks of the human leg throughout the step-cycle

154 showing that in humans the hip moves pendulously to ensure stability, while distal joints, particularly the ankle, generate
155 propulsion. Data are presented as mean±SEM, SEM is shown as shaded areas. N=6 for flies, N=9 for mice, N=29 for humans.

156 Next, we investigated how the same physiological perturbation, ageing, affects the execution
157 of locomotor programs across species. The PCA obtained with the AutoGaitA group-level analysis
158 indicates that the locomotor program shows an ageing signature in each species (Fig. 3a-c).
159 Remarkably, not all older subjects segregate from the "young cluster", showing inter-individual
160 variability in response to ageing in all species (Fig. 3a-c). To assess the components driving the
161 age-dependent adaptation of the locomotor programs, we analysed individual features next.
162 Intriguingly, and consistent with their species-specific roles in generating propulsion, we observed
163 that age reduced i) in flies, the flexion of the Fe-Ti and Cx-Tr angles at the swing-stance transition,
164 shortening the power stroke length (Fig. 3d, Supplementary Fig. 3a); ii) in mice, the extension of
165 the ankle at the swing-stance transition, affecting the knee/ankle dynamics driving the forward
166 thrust (Fig. 3e, Supplementary Fig. 3b); iii) in humans, the ankle flexion during stance that usually
167 provides the additional push-off power to move forward (Fig. 3f). Taken together, these
168 observations revealed a conserved effect of aging on locomotor programs: a reduction in the
169 generation of propulsive strength resulting from changes in the species-specific kinematic features
170 that underlie the forward thrust of the leg.

171

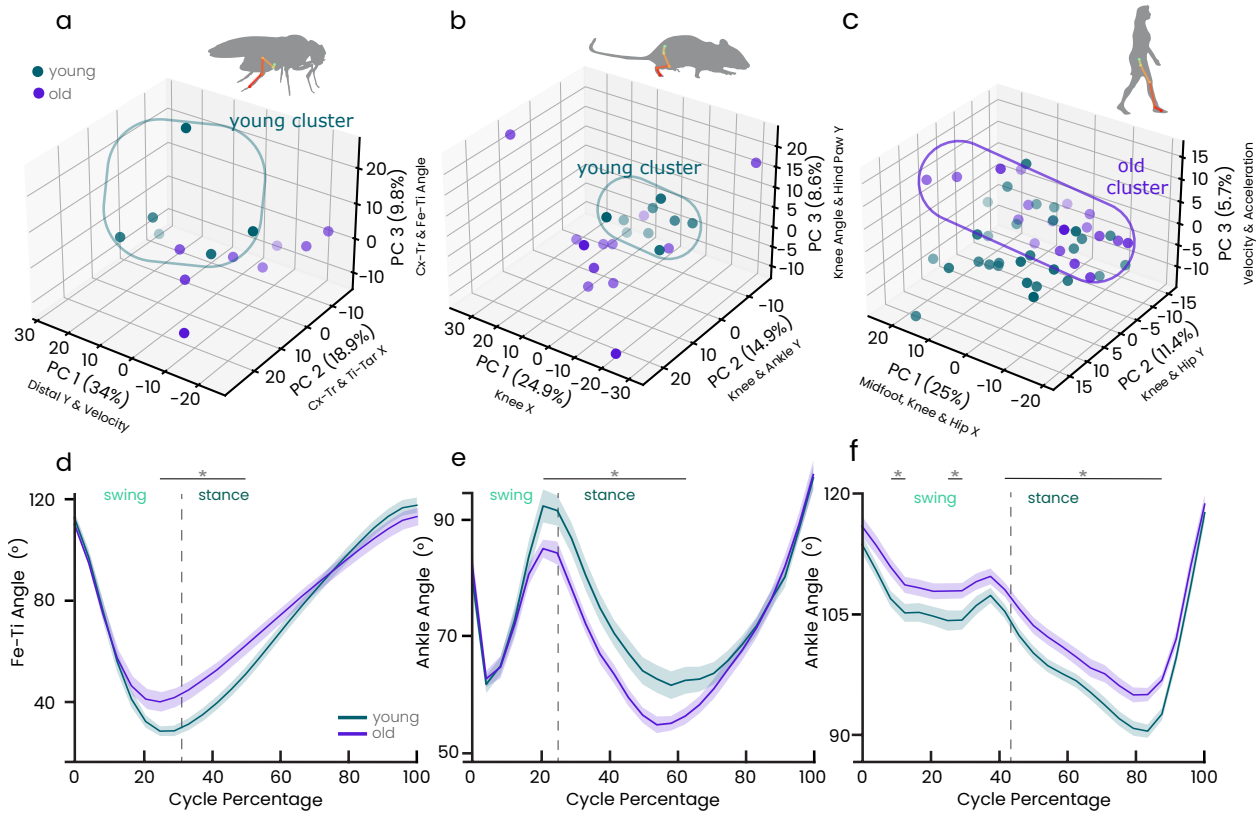

Figure 3 | Age-dependent adaptation of locomotor programs across species.
a, PCA scatterplot of fly posterior leg kinematics shows segregated clusters for young (green, 2-3 days, N=6) and old (purple, 21-22 days, N=6) flies. Each circle represents an individual fly. **b**, PCA scatterplot of mouse hindlimb kinematics shows segregated clusters for young (8 months, N=9) and old (24 months, N=12) mice. Each circle represents an individual mouse. **c**, PCA scatterplot of human leg kinematics shows partially segregated clusters for young (21-36 years, N=29) and old (46-85 years, N=18) humans. Each circle represents a single participant. **d**, Flexion of the femur-tibia (Fe-Ti) angle at the swing-stance transition is reduced in old compared to young flies. **e**, Extension of the ankle angle at the swing-stance transition is reduced in old compared to young mice. **f**, Flexion of the ankle angle during stance is reduced in old compared to young humans. Data are presented as mean±SEM, SEM is represented as shaded areas. Statistical analysis: one-way ANOVA followed by Tukey's post-hoc test. Significance is indicated with asterisks, *p<0.05. See Supplementary Tables S1-S9 for complete statistical and PCA results.

AutoGaitA accurately detects task- and age-dependent changes in mouse kinematics

Real-world locomotion rarely involves a single, discrete perturbation, but is rather influenced by multiple, simultaneous disturbances, whose effects add up to more than their sum. Thus, the nervous system must deploy adaptive motor programs that account for interactions between different perturbations. We therefore investigated how the adaptation of locomotor programs to

189 increased task difficulty evolves with age, studying how untrained 3-, 8-, and 24-month-old
190 C57BL6/J mice cross beams of varying widths: 25-, 12-, and 5-mm (Fig. 4a-4c).
191 3-month-old mice significantly changed their locomotor program to adapt to narrowing beams.
192 When mice crossed the 5-mm beam, the stride and the swing duration shortened (Fig. 4d). Further
193 during swing, the ankle and knee angles showed reduced flexion and increased extension (Fig.
194 4e,f), suggesting that mice walked with a predominantly extended limb posture, indicative of an
195 adaptive strategy to improve balance on a narrow surface. Importantly, hip kinematics were
196 unchanged (Fig. 4g), indicating that the requirement for increased precision of paw placement is
197 implemented mainly through a finer regulation of the distal joints. The challenge to balance on the
198 narrow beam caused the ankle/knee inversion, typically used to generate forward thrust, to be
199 reduced (Supplementary Fig. 4a-c), necessitating a compensatory increase in joint velocities to
200 generate sufficient propulsive strength (Supplementary Fig. 4d-f). Coalescing all meaningful
201 kinematic features (forelimb and hindlimb height, angles and velocity) in PCA space revealed
202 segregated clusters corresponding to the different beam widths (Fig. 4h). Thus, AutoGaitA's multi-
203 level analysis revealed the kinematic adaptation of locomotor programs to increased task difficulty.
204 Next, we investigated how age affects these locomotor adaptation strategies by comparing how
205 3- and 8-month-old mice performed on the beam task. Aging did not change the kinematic pattern
206 induced by the narrow beam, with older mice still showing reduced knee/ankle inversion
207 (Supplementary Fig. 4g-i), increased joint velocity (Supplementary Fig. 4j-l), shortened stride
208 (Supplementary Fig. 4m), less flexed ankle (Fig. 4i) and knee (Supplementary Fig. 4n), and no
209 changes to the hip angle (Supplementary Fig. 4n). However, 8-month-old mice adopted an even
210 more extended limb posture, with the ankle having higher peaks of extension at the end of swing
211 (Fig. 4i). Thus, 8-month-old mice preserve the ability to execute the 25-, 12-, and 5-mm locomotor

212 programs, but with minor adjustments, such as increased distal joint extension (Fig. 4i,
213 Supplementary Fig. 4g-n). Consistently, the PCA showed that the 25-, 12-, and 5-mm locomotor
214 programs cluster separately, but with almost no difference between ages (Supplementary Fig. 4o).
215 Finally, we compared 8- and 24-month-old mice on the beam task. Age reduced paw placement
216 dexterity, with older mice displaying increased footslips (Supplementary Fig. 5a). Nevertheless,
217 the kinematic adaptation to narrower beams was preserved, as older mice still exhibited shortened
218 stride (Fig. 4j), extended leg posture (Fig. 4k, Supplementary Fig. 5d-f), and increased joint
219 velocity (Supplementary Fig. 5g-i). In contrast to younger mice, 24-month-old mice displayed
220 increased hip flexion on the 5-mm beam (Supplementary Fig. 5c), suggesting a more crouched
221 posture to lower the centre of mass and improve postural stability. This crouched posture was also
222 evident when comparing 8- and 24-month-old mice, as older mice exhibited a reduced peak of
223 ankle extension during swing (Fig. 4k). Finally, the PCA showed a clear separation by both age
224 and beam width (Fig. 4l), suggesting that locomotor programs undergo a more significant change
225 between 8 and 24 months than at earlier stages (Supplementary Fig. 4o).
226 In summary, AutoGaitA enabled us to identify task-specific locomotor programs, and assess
227 how they change as a function of age.

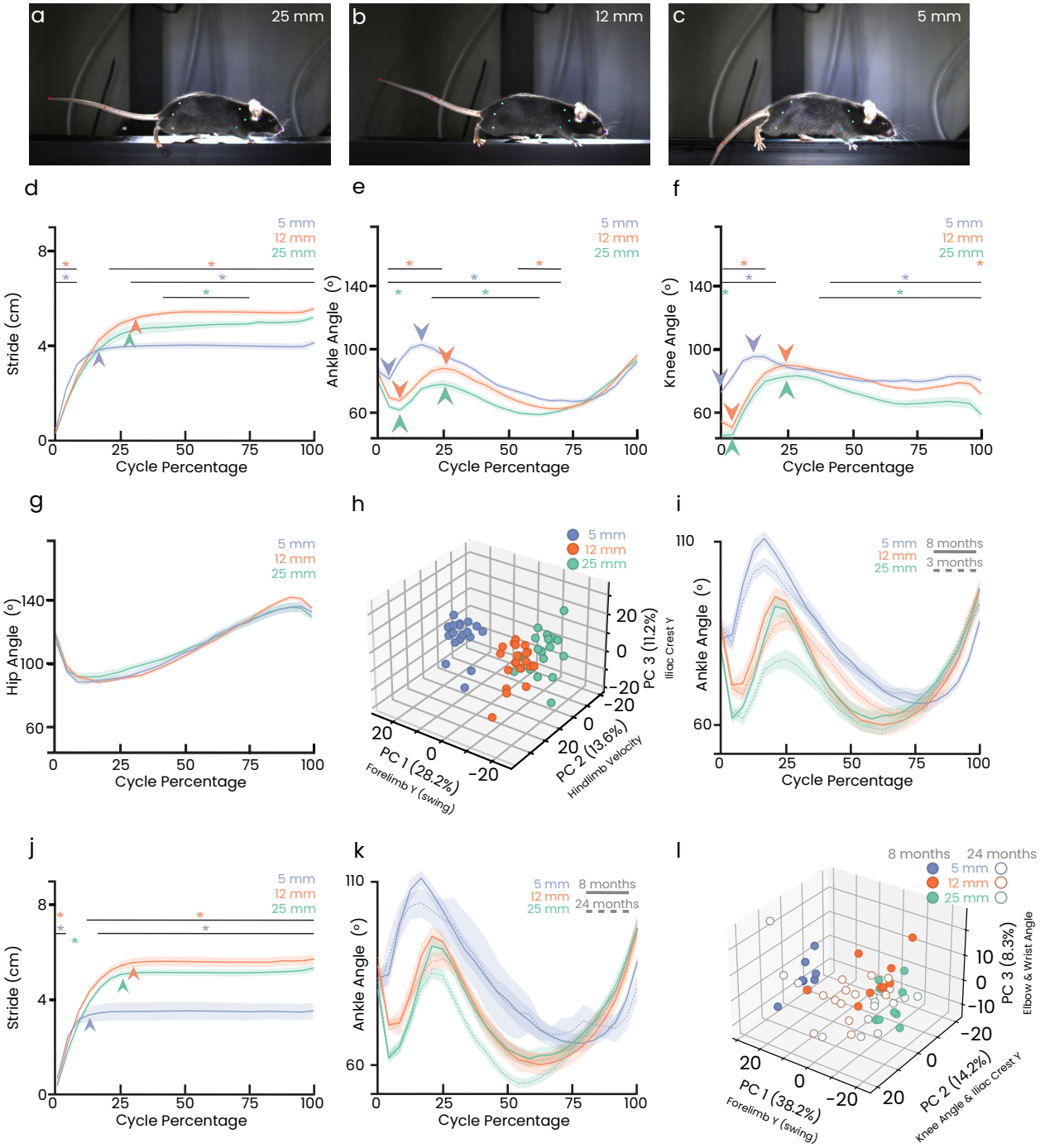

Figure 4 | Task- and age-dependent motor adaptation of locomotor programs in mice.
a-c, Snapshots of a mouse crossing the 25 mm (a), 12 mm (b) and 5 mm (c) wide beam. **d**, 3-month-old mice shorten their stride when crossing a 5 mm wide beam (blue) compared to the 25 mm (green) and 12 mm (orange) wide beams. The shortened stride also corresponds to a shorter swing, as indicated by the arrowheads coloured according to beam widths. **e-g** Changes during the step cycle in the ankle (e), knee (f) and hip (g) angles in 3-month-old mice crossing the 25 mm (green), 12 mm (orange) and 5 mm (blue) wide beams. Mice crossing the narrowest (5 mm) beam showed reduced flexion and increased extension of the ankle and knee during swing, as indicated by the coloured arrowheads. **h**, PCA of changes in heights, angles and velocities of the forelimb and hindlimb throughout the step cycle revealed segregated clusters based on beam widths. Each circle represents an individual mouse. **i**, Ankle angles of 8-month-old (solid lines) and 3-month-old (dashed lines) mice crossing

the three beams. 8-month-old mice exhibited a similar kinematic pattern of beam-induced adaptation, but an even more accentuated extended-limb posture. **j**, 24-month-old mice shorten their stride even more when crossing a 5 mm wide beam (blue) compared to the 25 mm (green), 12 mm (orange) wide beams. The shortened stride also corresponds to a shorter swing, as indicated by the arrowheads coloured according to beam widths. **k**, Ankle angles of 8-month-old (solid lines) and 24-month-old (dashed lines) mice crossing the three beams. 24-month-old mice exhibited a similar kinematic pattern of beam-induced adaptation, but flexed their joints more, indicating a crouched position on the beam to lower their centre of mass. **l**, PCA of changes in heights, angles and velocities of the forelimb and hindlimb throughout the step cycle between 8-month-old (solid lines) and 24-month-old (dashed lines) mice revealed segregated clusters based on beam widths and age. Each circle represents an individual mouse. Data presented as mean±SEM. N=20 for 3-month-old, N=9 for 8-month-old and N=12 for 24-month-old mice. Statistical comparison: one-way ANOVA followed by Tukey's post-hoc test, significance is indicated by orange (5-mm versus 12-mm), blue (5-mm versus 25-mm), and green (12-mm versus 25mm) asterisks. See Supplementary Tables S10-S20 for complete statistical and PCA results.

Discussion

We have developed AutoGaitA, the open-source Python toolbox providing a versatile framework for the quantitative and standardised assessment and comparison of motor programs at different levels of granularity across species and behaviours. Showcasing the potential of this framework, we used it to reveal three key principles in motor control: i) the species-specific biomechanics underlying propulsive strength generation during walking (Fig. 2); ii) the age-dependent adaptation mechanisms to generate propulsive strength (Fig. 3); iii) the combined effects that concomitant perturbations exert on locomotor programs to preserve robustness and flexibility (Fig. 4).

A versatile quantitative framework for motor control

One of the key factors underlying the deep-learning posture tracking revolution has been the algorithms´ applicability to any species or task[4,5]. We have developed a similarly versatile tool that enables comparable and standardised kinematic outputs to be generated independently of the input. This versatility has already been leveraged to identify gait alterations in cerebellar neurodegeneration[18], assess to which extent physiological locomotor programs are restored in a mouse model of ataxia[19], and characterise how perturbations of spinal interneurons affect limb movement in neonatal mice[20].

AutoGaitA can also be used to assess the motor programs underlying other rhythmic behaviours, such as those commonly used as readouts of dexterity (rope pulling, ladder walking) or deregulated sensation (grooming, chronic scratching). Compiling kinematic data of all these behaviours with AutoGaitA will establish a catalogue of motor programs across model organisms. Moreover, the annotation tables provide an additional tool to compare successful to failed cycles or failed cycles across mutations or perturbations, granting important insight into how motor

273 programs are adapted or degraded by physiological and pathological states. The standardised
274 comparison of motor programs in health and disease will allow to better classify motor disorders,
275 to identify motor symptom progression over the course of diseases and to unveil early disease
276 hallmarks in pre-symptomatic stages.

277 Beyond, future applications of AutoGaitA could involve assessing athletes' performance in
278 sports science, optimising treatments in physiotherapy and neurology, studying the impact of
279 affective disorders on motor behaviours in psychiatry, and establishing kinematic readouts of
280 environmental influences (e.g. stress/anxiety) in behavioural research.

281 **Propulsion in locomotion: species-, age- and task-dependent mechanisms**

282 The generation of propulsion during locomotion varies widely across species, reflecting
283 differences in biomechanical constraint, body size, and environmental demands[21]. In hexapedal
284 organisms such as fruit flies, posterior leg propulsion relies on the synchronised flexion and
285 extension of all distal leg joints, producing a coordinated power stroke that drives forward
286 movement (Fig. 2g,j, Supplementary Fig. 2a,d). Quadrupedal mammals such as mice use a hip-
287 driven initial power stroke, while the coordinated but opposing ankle and knee movements create
288 the primary thrust (Fig. 2h,k, Supplementary Fig. 2b,e). In contrast, humans combine hip
289 oscillations with ankle push-offs, with the ankle generating additional power during the stance-to-
290 swing transition (Fig. 2i,l, Supplementary Fig. 2c,f). Taken together, our data show how evolution
291 has shaped distinct kinematic solutions to the fundamental challenge of efficient forward
292 propulsion of the leg. Notably, in multi-legged species, interlimb coordination is required to
293 preserve postural stability and synergise the propulsion generated by individual limbs[1].

294 Ageing degrades locomotor ability in all species by causing declines in muscle strength, joint
295 flexibility, and neural control[22–24]. Yet, whether the age-dependent changes in locomotor programs

296 follow convergent or divergent mechanisms across species has been a long-standing open question.
297 Difficulties in addressing this question arise from studies focusing on different outputs – strength,
298 stride, coordination, endurance, dexterity – and results needing to be evaluated in light of the
299 distinct biomechanics. By using comparable paradigms and standardised readouts, we determined
300 a conserved mechanism of age-dependent locomotor adaptation in flies, mice and humans: the
301 decline of propulsive strength (Fig. 3). This decline manifested within the constraints of each
302 species' unique biomechanics (Fig. 3). Defining the mechanistic bases underlying the ageing
303 decline of propulsive strength is particularly important with respect to the motor impairments
304 caused by neurodegenerative diseases and for establishing meaningful comparisons between
305 patients and animal models. For example, ankle push-off power is decreased in ageing humans
306 (Fig. 3f)[25,26], especially in stroke patients[27]. However, our findings imply that in a mouse model of
307 stroke, the loss of propulsive strength should be studied with a focus on the knee/ankle inversion
308 instead of the ankle push-off.

309 When locomotor tasks become more demanding, such as crossing narrow paths, the nervous
310 system has to balance stiffness and forward propulsion in a way that guarantees postural stability[28].
311 As mice cross narrow beams, hindlimbs become rather stiff, with propulsive strength being
312 generated by faster joint movements instead of the typical large angular excursions (Fig. 4a-f,
313 Supplementary Fig. 4a-f). We additionally showed that as mice age and require an even finer
314 balance control, this alternative strategy to generate propulsion was complemented by a lower
315 centre of mass (Fig. 4k, Supplementary Fig. 5).

316 In summary, AutoGaitA represents a much-needed standardized framework for the quantitative
317 assessment of motor programs across behaviours, perturbations, and species. Through our
318 showcase studies, we demonstrated that AutoGaitA enables the discovery of fundamental

principles governing motor control across species. We anticipate that this framework will have profound implications for advancing therapeutic interventions, optimizing rehabilitative strategies, and elucidating the evolutionary basis of motor control.

Acknowledgements

We thank Nicholas Del Grosso (iBots, University of Bonn) for help with research software engineering, Prof. Kathrin Möllenhoff (University of Cologne) for consulting on the appropriate statistical analysis, and the student assistants Sarah Sabbagh and Luca Flemming for their contributions to the code. This work was funded by the Deutsche Forschungsgemeinschaft (DFG, German Research Foundation) - SFB 1451 Project-ID 431549029-INF, 431549029-Z02, 431549029-Z03. M.Ha., A.B., I.K. and G.G. are members of the "iBehave" network funded by the Ministry of Culture and Science of the State of North Rhine-Westphalia.

Author contribution

Conceptualisation: M.H., I.K., A.G., S.D. and G.G.; data curation: M.H., I.K., V.W., C.S., T.D.K., M.Ha.; analysis: M.H., I.K., V.W., A.K., M.T., M.Ha.; investigation: M.H., I.K., V.W., M.Ha., C.S., T.D.K., V.M., A.G.; methodology: M.H., I.K., V.W., M.Ha., S.D., G.G.; resources: T.K., A.B., P.H.W., C.G., G.R.F., S.D., G.G.; software: M.H.; supervision: T.K., A.B., P.H.W., G.R.F., S.D., G.G.; validation: M.H., I.K., V.W., M.Ha., M.T., G.G.; visualisation: M.H., G.G.; writing of the original draft: M.H., G.G.; reviewing and editing: M.H., I.K., V.W., C.S., T.D.K., V.M., M.Ha., M.T., T.K., A.B., C.G., P.H.W., G.R.F., S.D., G.G.

Methods

Software Availability

AutoGaitA is provided as an open-source Python toolbox (GitHub – mahan-hosseini/AutoGaitA: Automated Gait Analysis in Python), being developed on top of well established, documented, and maintained Python dependencies: NumPy[29,30] (https://numpy.org), SciPy[31] (https://scipy.org), pandas[32] (https://pandas.pydata.org), Scikit-Learn[33] (https://scikit-learn.org), Pingouin[34] (https://pingouin-stats.org/), Matplotlib[35] (https://matplotlib.org), seaborn[36] (https://seaborn.pydata.org), CustomTkinter (https://customtkinter.tomschimansky.com), Pillow[37] (https://python-pillow.github.io), openpyxl (https://openpyxl.readthedocs.io/en/stable/), ffmpeg-python (https://kkroening.github.io/ffmpeg-python/), and h5py[38] (https://www.h5py.org).

AutoGaitA's source code can be accessed in the GitHub repository under the GPLv3 license, and is further integrated with Zenodo[39] (http://doi.org/10.5281/zenodo.15373063), automatically linking all releases to unique digital object identifiers (DOIs). AutoGaitA's central goal is to take off the burden of post-tracking analyses from researchers, particularly those not too familiar with programming. We thus provide easy-to-understand graphical user interfaces (GUIs), a straightforward documentation consisting of many images, and comprehensive video tutorials on the AutoGaitA YouTube channel. Nonetheless, we have simultaneously made it easy for well-versed developers and users to contribute to and extend AutoGaitA as well as to integrate our toolbox into custom workflows and other (Python) tools. We strongly appreciate and encourage user feedback and contributions via email: autogaita@fz-juelich.de or directly as GitHub pull requests.

361 ***AutoGaitA workflow details***

362 **Data preparation and important settings**

363 For AutoGaitA DLC and SLEAP, we provide two ways of naming input data files: a thorough
364 and safe way, which provides detailed information about the contents of files, and a reduced and
365 risky way, which is quick to implement but carries some ambiguity. AutoGaitA Universal 3D
366 includes a tool which allows convenient adaptation of the required naming convention of the
367 columns of corresponding 3D data files. Since AutoGaitA Universal 3D analyses 2D kinematics
368 of 3D body coordinates, users are advised to pay attention to their behaviour of interest and to
369 which dimension's features are of particular interest (e.g. along which 2D-plane angles should be
370 computed). Excel tables containing the timestamp annotations of the behaviour to be analysed
371 (annotation tables) need to be prepared before any analysis. These need to follow a specific format,
372 which differs slightly between AutoGaitA DLC/SLEAP and AutoGaitA Universal 3D.

373 **Normalisation of segmented data**

374 In first-level workflows (Figure 1b), segmented data is normalised to be equally long for all
375 cycles. In the explanations below, we will use *time-points* when referring to the length of original
376 cycles before normalisation and *cycle-bins* when referring to the length of normalised cycles.
377 Cycles are normalised to a user-chosen target length n (in cycle-bins) by being either extended if
378 they were shorter (i.e. had fewer time-points than n originally) or compressed if they were longer
379 (i.e. had more time-points than n originally). For example, if the user selected to normalise to ten
380 cycle-bins, all original cycles of length 9 or below would be extended, and all original cycles of
381 length 11 or more would be compressed. Extension is done via repetition. For the example target
382 value of 10 cycle-bins and an original cycle having only 5 time-points before normalisation, all its
383 data values will be repeated once (i.e.: original data at time-points: 1, 1, 2, 2, … 5, 5 = normalised

384 data at cycle-bins 1, 2, 3, 4, … 9, 10). Compression is done via averaging. In our example, if the
385 original cycle comprises 20 time-points, its data points are averaged in adjacent pairs: first and
386 second, third and fourth data points and so on (i.e.: averages of data at time-points: 1 & 2, 3 & 4,
387 5 & 6, 7 & 8, … 17 & 18, 19 & 20 = normalised data at cycle-bins 1, 2, 3, …, 9, 10).

388 After normalisation, each cycle-bin thus represents the data at respective percentiles, based on
389 the number of selected bins. Default settings normalise to 25 cycle-bins, leading to cycle-bins
390 reflecting 4% percentiles: 1-4%, 5-8%, 9-12%, etc., since this value showed the best comparability
391 in our cross-species locomotion analysis.

392 **Standardisation of direction of movement**

393 In the same locomotion experiment, animals might walk through the video screen from left to
394 right or vice versa. To ensure that the data is independent of the direction of motion, AutoGaitA
395 offers options to adjust the horizontal coordinates (e.g., x-coordinates in 2D), effectively
396 simulating that all animals walk towards the same point. For behaviours like jumping jacks or rope
397 climbing, which are approximately stationary along the horizontal dimension, this option should
398 be turned off. Users of AutoGaitA Universal 3D should consider additional details about this
399 standardisation in 3D in the documentation's section on *back and forth behaviours*.

400 **Standardisation of horizontal coordinates**

401 AutoGaitA provides an option to analyse horizontal coordinates, for example, x-coordinates in
402 2D (see Fig. 4d). In a locomotion study, the x-coordinates of the foot inform about its distance
403 travelled with each step (i.e., the stride). To ensure that x-coordinates are comparable across steps,
404 they must be standardised to the same position across cycles. This standardisation ensures that no
405 bias is introduced by AutoGaitA averaging features across cycles (and, consecutively, across
406 animals at the group level). For standardisation, we subtract, at each cycle separately, the minimum

407 x-coordinate of a user-chosen key point from those of all key points. As a result, x-coordinates
408 after standardisation inform about key points' distance to the standardisation-joint's zero-point and
409 are, critically, independent of their absolute position in space.

410 **Standardisation of vertical coordinates**

411 Vertical coordinates, for example y-coordinates in 2D, can be standardised according to
412 baseline, global, or landmark standardisation. In the (typically most accurate) baseline
413 standardisation, the y-coordinates of a tracked reference baseline, like the beam in our mouse
414 experiments (Fig. 2b), are subtracted from those of the animal's body at the corresponding time
415 points. If no baseline data is available, users can use global or landmark standardisation. Global
416 standardisation subtracts the smallest y-coordinate present across the full dataset (i.e., across time
417 and all landmarks) from the y-coordinates of all body landmarks. Landmark standardisation
418 subtracts the smallest y-coordinate of a user-chosen landmark from the body's y-coordinates.
419 AutoGaitA also provides an option to standardise the y-coordinates of each step separately, which
420 is recommended if no baseline standardisation is possible and the floor is uneven or cameras are
421 distorted.

422 **Principal Components Analysis**

423 Users can choose which kinematic features to include in AutoGaitA's Principal Components
424 Analysis (PCA), which commences with extracting averages of these features across the entire
425 cycle for each animal (Fig. 1c). Each cycle-bin of each feature is included as an input feature in
426 the PCA. For example, if the ankle angle is an input feature and cycles were normalised to 10
427 cycle-bins, the PCA would have 10 input features capturing animals' ankle angles: ankle angle 1-
428 10% cycle, ankle angle 11-20% cycle, …, ankle angle 91-100% cycle. Users have the option to
429 compute input features only over a subset of the cycle (e.g. the first half, or the first and last

430 quartile) instead. Following the PCA convention, input features are standardised to have zero mean
431 and unit variance before the model is fitted. Scikit-Learn[33] is used for standardisation as well as
432 model-fitting. Depending on user input, the number of returned principal components (PC) can
433 either be chosen directly or configured to explain a certain percentage of data variance. AutoGaitA
434 produce5s PCA outputs as: 2D- and 3D scatterplots, generating video-files of the latter if wanted,
435 and tabular files containing PC's explained variance, input features' eigenvectors, each animal's
436 coordinates in PC-space, and an overview of the 20 input features that contributed most strongly
437 to each PC to simplify their interpretability.

438 **One-way ANOVA and Tukey's Test**

439 AutoGaitA provides between- or within-subjects one-way ANOVAs, with the former assessing
440 different subjects, as in Fig. 3, and the latter assessing the same subjects across different conditions,
441 as in Fig. 4d-f, for example. ANOVA results are provided as conventional ANOVA tables in text
442 files. While the one-way ANOVA tests a certain feature for group differences globally, Tukey's
443 post-hoc test compares the feature at individual cycle-bins separately, correcting for the number
444 of multiple comparisons (AutoGaitA does not require the ANOVA for Tukey's to be run). Besides
445 figures illustrating the results of Tukey's tests, we provide their exact numerical results (i.e.,
446 Tukey's q-values as well as corresponding p-values and confidence intervals) in text and tabular
447 files. AutoGaitA uses Pingouin[34] for one-way ANOVAs and SciPy[31] for Tukey's tests.

448 **Cluster-extent Permutation Test**

449 The cluster-extent test is preferred over the ANOVA whenever parametric assumptions are not
450 met. AutoGaitA's cluster-extent test follows the concepts introduced by Maris and Oostenveld[40],
451 which are by now well-established in the field of human electrophysiology. We provide an in-
452 depth explanation of how the test is implemented in AutoGaitA in Hosseini et al.[41]. The outputs of

453 the cluster-extent test are provided as figures as well as text files, storing the p-values of all clusters.
454 AutoGaitA uses SciPy[31] for t-tests and Scikit-Learn[33] for shuffling data randomly.

455 ***Experimental fly model***

456 Adult male wild-type Canton-S *Drosophila melanogaster* flies were collected after eclosion
457 and reared on a standard yeast-based medium[42] at 25°C and 65% humidity in a 12-hour dark/light
458 cycle. Experiments were performed with young (2-3 days old) and old (21-22 days old) flies.
459 Tethered flies walked on a spherical treadmill and were recorded from the side using a high-speed
460 camera (acA1300-200um, Basler), equipped with a 50 mm lens (LM50JC1MS, Kowa Optical
461 Products)[12]. Videos were recorded at 400 frames/second with a resolution of 912 x 550 pixels. To
462 convert pixels into metric scale, the camera was calibrated with a custom-made checkerboard
463 pattern (7 x 6 squares with size 399 µm x 399 µm per square) developed on a photographic slide.
464 The conversion factor of 5.883 ± 0.198 µm per pixel (mean ± standard deviation) was determined
465 by analysing the side length of 1850 squares from 74 images of the checkerboard.

466 DeepLabCut[4] was used for automated tracking of leg landmarks in the videos by training a
467 ResNet-50 network with a training set containing 755 images (10 videos with 54 to 105 frames
468 each) from 5 flies. Resulting leg landmark predictions were visually inspected and manually
469 corrected as needed with a custom-made graphical user interface software. Begin and end times
470 for swing and stance phases were manually annotated for each step.

471 ***Experimental mouse model***

472 Mice were maintained following the protocols for animal experiments approved by the local
473 health authority in North Rhine-Westphalia (LAVE, Landesamt für Verbraucherschutz und
474 Ernährung, Nordrhein-Westfalen). 3-month-, 8-month- and 24-month-old C56BL6/J mice of both
475 sexes were used for behavioural experiments. These mouse age groups are commonly used to

476 characterise gait following physiological, pathological and circuit perturbations. Analysis of the
477 behavioural data showed similar responses in male and female mice. Mice had *ad libitum* access
478 to food and water, and were housed in groups of maximum 5 animals, maintained on a 12-hour
479 dark/light cycle within a room controlled for humidity and temperature.

480 We opted for the beam paradigm to test a challenge, e.g. walking on a narrowing path, mice
481 are likely to encounter also in their naturalistic settings. Naïve mice of different ages were tested
482 as they crossed 1.3-meter-long beams with different widths (5-mm, 12-mm, and 25-mm). Studying
483 untrained mice enables the identification of innate adaptation strategies in response to the width-
484 dependent perturbations. On the first day, mice were tasked to cross the wide, 25-mm, beam, on
485 the second day the 12-mm beam, and on the third day the narrow, 5-mm, beam. For each beam
486 size, three to five trials per mouse were recorded using eight high-speed cameras (mV Blue Cougar
487 XD) positioned around the beam (3D Simi Motion). Multiple camera views were analysed to count
488 the number of slips, which were then averaged across trials per individual mouse. Videos were
489 recorded at 100 frames/second, with a resolution of 1200 x 900 pixels.

490 The Simi™ Motion software (version 10.2.0) was used to record markerless mice walking in
491 both directions, so our data are averages of both right and left limbs. We used DeepLabCut[4] to
492 track the body landmark coordinates, as well as the beam surface to define our vertical baseline.
493 Tracking was done after training a ResNet-50 network on 2147 frames (113 videos with 19 frames
494 each) from 8 mice. The number of slips and the phases of the step cycle (beginning of swing, end
495 of swing, and end of stance) were manually annotated. Slips or pauses on the beam were excluded
496 from the kinematic analysis. Please note that 24-month-old mice display an increased number of
497 slips on the narrowest beam (5-mm), thus, we analysed fewer animals compared to the other tasks.

498 ***Human dataset***

499 Participants meeting the following criteria were eligible for inclusion in the study: Age
500 between 21 and 90 years, written informed consent, absence of neurological or psychiatric diseases
501 and no health conditions affecting the locomotor system. The study was conducted according to
502 the principles of the Declaration of Helsinki and approved by the local ethics committee of the
503 Faculty of Medicine at University of Cologne (21-1418_1). The final sample is presented in
504 Supplementary Table S32 and consisted of 47 individuals, including 29 younger participants (age
505 [mean ± SD]: 28.1 ± 3.5 years, age range: 21 to 36 years; 19 females) and 18 older participants
506 (age [mean ± SD]: 67.7 ± 11.0 years, age range: 46 to 85; 9 females). There were no significant
507 differences between the two age groups with regard to sex ($\chi^2 = 0.560$, $p = 0.454$) and body height
508 ($t = 0.819$, $p = 0.417$).

509 Participants walked on a walkway (460 cm in length x 60 cm in width), while being recorded
510 by eight high-speed cameras (mvBlueCougar XD, Matrix Vision GmbH) positioned in a circular
511 arrangement around the walkway. Videos were recorded at 100 frames/second, with a resolution
512 of 1936 x 1216 pixels. The Simi™ Motion software (version 10.2.0) was used for the video
513 recordings and DeepLabCut[4] was used to track body landmarks. Tracking was done after training
514 a ResNet-50 network on 4797 frames (123 videos with 39 frames each) from 31 humans.

515 At the beginning of the recordings, participants were asked to stand at a marked position on
516 one end of the walkway. After a verbal signal, participants started walking at a convenient, self-
517 generated speed to the other end of the walkway. Once they arrived at the end, they turned around
518 and walked back to the start position. This back-and-forth walking was repeated until up to three
519 trials were performed by each participant. Videos were split based on turns before being tracked
520 with DLC, meaning that (as for our mouse data) the data corresponds to averages of left and right

legs. Step cycle phases, i.e., the start of the swing phase, the end of the swing phase, and the end of the stance phase, were annotated manually. More specifically, the toe-off moment of the feet was marked as the end of the stance phase and simultaneously as the start of the swing phase, while the moment of the heel-strike was marked as the end of the swing phase and simultaneously as the start of the stance phase.

References

1. Büschges, A. & Ache, J. M. Motor control on the move: from insights in insects to general mechanisms. *Physiol. Rev.* **105**, 975–1031 (2025).
2. Grillner, S. & El Manira, A. Current Principles of Motor Control, with Special Reference to Vertebrate Locomotion. *Physiol. Rev.* **100**, 271–320 (2020).
3. Bernstein, N. *The Co-Ordination and Regulation of Movements*. (Pergamon Press; Oxford, 1967).
4. Mathis, A. *et al.* DeepLabCut: markerless pose estimation of user-defined body parts with deep learning. *Nat. Neurosci.* **21**, 1281–1289 (2018).
5. Pereira, T. D. *et al.* SLEAP: A deep learning system for multi-animal pose tracking. *Nat. Methods* **19**, 486–495 (2022).
6. Aljovic, A. *et al.* A deep learning-based toolbox for Automated Limb Motion Analysis (ALMA) in murine models of neurological disorders. *Commun. Biol.* **5**, 131 (2022).
7. Lv, X. *et al.* PMotion: an advanced markerless pose estimation approach based on novel deep learning framework used to reveal neurobehavior. *J. Neural Eng.* **20**, 046002 (2023).
8. Tozzi, F., Zhang, Y.-P., Narayanan, R., Roquiero, D. & O'Connor, E. C. Forestwalk: A machine learning workflow brings new insights into posture and balance in rodent beam walking. *bioRxiv* 2024.04.26.590945 (2024) doi:10.1101/2024.04.26.590945.
9. Ruiz-Vitte, A. *et al.* Ledged Beam Walking Test Automatic Tracker: Artificial intelligence-based functional evaluation in a stroke model. *Comput. Biol. Med.* **186**, 109689 (2025).
10. Chockley, A. S. *et al.* Subsets of leg proprioceptors influence leg kinematics but not interleg coordination in *Drosophila melanogaster* walking. *J. Exp. Biol.* **225**, jeb244245 (2022).

548 11. DeAngelis, B. D., Zavatone-Veth, J. A. & Clark, D. A. The manifold structure of limb
549 coordination in walking Drosophila. *eLife* **8**, e46409 (2019).
550 12. Haustein, M., Blanke, A., Bockemühl, T. & Büschges, A. A leg model based on anatomical
551 landmarks to study 3D joint kinematics of walking in Drosophila melanogaster. *Front.*
552 *Bioeng. Biotechnol.* **12**, 1357598 (2024).
553 13. Pratt, B. G., Lee, S.-Y. J., Chou, G. M. & Tuthill, J. C. Miniature linear and split-belt
554 treadmills reveal mechanisms of adaptive motor control in walking Drosophila. *Curr. Biol.*
555 **34**, 4368-4381.e5 (2024).
556 14. Bellardita, C. & Kiehn, O. Phenotypic Characterization of Speed-Associated Gait Changes in
557 Mice Reveals Modular Organization of Locomotor Networks. *Curr. Biol.* **25**, 1426–1436
558 (2015).
559 15. Takeoka, A., Vollenweider, I., Courtine, G. & Arber, S. Muscle Spindle Feedback Directs
560 Locomotor Recovery and Circuit Reorganization after Spinal Cord Injury. *Cell* **159**, 1626–
561 1639 (2014).
562 16. Gonzalez-Islas, J. C., Dominguez-Ramirez, O. A., Castillejos-Fernandez, H. & Castro-
563 Espinoza, F. A. Human gait analysis based on automatic recognition: A review. *Pädi Bol.*
564 *Científico Cienc. Básicas E Ing. ICBI* **10**, 13–21 (2022).
565 17. Ghorbani, S. *et al.* MoVi: A large multi-purpose human motion and video dataset. *PLOS*
566 *ONE* **16**, e0253157 (2021).
567 18. Tolve, M. *et al.* The endocytic adaptor AP-2 maintains Purkinje cell function by balancing
568 cerebellar parallel and climbing fiber synapses. *Cell Rep.* **44**, (2025).
569 19. Tutas, J. *et al.* Autophagy regulator ATG5 preserves cerebellar function by safeguarding its
570 glycolytic activity. *Nat. Metab.* **7**, 297–320 (2025).

20. Trevisan, A. J. *et al.* The transcriptomic landscape of spinal V1 interneurons reveals a role for En1 in specific elements of motor output. Preprint at https://doi.org/10.1101/2024.09.18.613279 (2024).
21. Schaeffer, P. J. & Lindstedt, S. L. How Animals Move: Comparative Lessons on Animal Locomotion. in *Comprehensive Physiology* (ed. Prakash, Y. S.) 289–314 (Wiley, 2013). doi:10.1002/cphy.c110059.
22. Desforges, J. F. & Sudarsky, L. Gait Disorders in the Elderly. *N. Engl. J. Med.* **322**, 1441–1446 (1990).
23. Ingram, D. K., London, E. D., Reynolds, M. A., Waller, S. B. & Goodrick, C. L. Differential effects of age on motor performance in two mouse strains. *Neurobiol. Aging* **2**, 221–227 (1981).
24. Jones, M. A. & Grotewiel, M. Drosophila as a model for age-related impairment in locomotor and other behaviors. *Exp. Gerontol.* **46**, 320–325 (2011).
25. Franz, J. R. The Age-Associated Reduction in Propulsive Power Generation in Walking. *Exerc. Sport Sci. Rev.* **44**, 129–136 (2016).
26. Sloot, L. H. *et al.* Decline in gait propulsion in older adults over age decades. *Gait Posture* **90**, 475–482 (2021).
27. Balasubramanian, C. K., Bowden, M. G., Neptune, R. R. & Kautz, S. A. Relationship Between Step Length Asymmetry and Walking Performance in Subjects With Chronic Hemiparesis. *Arch. Phys. Med. Rehabil.* **88**, 43–49 (2007).
28. Earhart, G. M. Dynamic control of posture across locomotor tasks. *Mov. Disord.* **28**, 1501–1508 (2013).
29. Harris, C. R. *et al.* Array programming with NumPy. *Nature* **585**, 357–362 (2020).

30. Van Der Walt, S., Colbert, S. C. & Varoquaux, G. The NumPy Array: A Structure for Efficient Numerical Computation. *Comput. Sci. Eng.* **13**, 22–30 (2011).
31. Virtanen, P. *et al.* SciPy 1.0: fundamental algorithms for scientific computing in Python. *Nat. Methods* **17**, 261–272 (2020).
32. McKinney, W. Data Structures for Statistical Computing in Python. in 56–61 (Austin, Texas, 2010). doi:10.25080/Majora-92bf1922-00a.
33. Pedregosa, F. *et al.* Scikit-learn: Machine Learning in Python. *J Mach Learn Res* **12**, 2825–2830 (2011).
34. Vallat, R. Pingouin: statistics in Python. *J. Open Source Softw.* **3**, 1026 (2018).
35. Hunter, J. D. Matplotlib: A 2D Graphics Environment. *Comput. Sci. Eng.* **9**, 90–95 (2007).
36. Waskom, M. seaborn: statistical data visualization. *J. Open Source Softw.* **6**, 3021 (2021).
37. Murray, Andrew *et al.* python-pillow/Pillow: 11.2.1. Zenodo https://doi.org/10.5281/ZENODO.596518 (2025).
38. Collette, A. *Python and HDF5: Unlocking Scientific Data*. (O'Reilly, Beijing Köln, 2014).
39. Hosseini, M. AutoGaitA - Automated Gait Analysis in Python. Zenodo https://doi.org/10.5281/ZENODO.15373063 (2025).
40. Maris, E. & Oostenveld, R. Nonparametric statistical testing of EEG- and MEG-data. *J. Neurosci. Methods* **164**, 177–190 (2007).
41. Hosseini, M. *et al.* AutoGaitA – Automated Gait Analysis in Python. *bioRxiv* 2024.04.14.589409 (2024) doi:10.1101/2024.04.14.589409.
42. Backhaus, B.S.E., Sulkowski, E. & Schlote, F.W. A semi-synthetic, general-purpose medium for Drosophila melanogaster. in *Drosophila Information Service* vol. 60 210–212 (1984).